11-16-2001

# In-cloud oxidation of SO2 by O3 and H2O2: Cloud Chamber Measurements and Modeling of Particle Growth

Peter F. Caffrey
*Naval Research Laboratory*

William Hoppel
*Naval Research Laboratory*

Glendon Frick
*Naval Research Laboratory*

Louise Pasternack
*Naval Research Laboratory*

James Fitzgerald
*Naval Research Laboratory*

***See next page for additional authors***

## NSUWorks Citation

Caffrey, P. F., Hoppel, W., Frick, G., Pasternack, L., Fitzgerald, J., Hegg, D. A., Gao, S., Leaitch, W. R., Shantz, N., Albrechcinski, T., & Ambrusko, J. (2001). In-cloud oxidation of SO2 by O3 and H2O2: Cloud Chamber Measurements and Modeling of Particle Growth. Journal of Geophysical Research: Atmospheres, 106, (D21), 27587 - 27601. https://doi.org/10.1029/2000JD900844. Retrieved from https://nsuworks.nova.edu/cnso_chemphys_facarticles/140

**Authors**
Peter F. Caffrey, William Hoppel, Glendon Frick, Louise Pasternack, James Fitzgerald, Dean A. Hegg, Song Gao, W. R. Leaitch, Nicole Shantz, Thomas Albrechcinski, and John Ambrusko

JOURNAL OF GEOPHYSICAL RESEARCH, VOL. 106, NO. D21, PAGES 27,587-27,601, NOVEMBER 16, 2001

# In-cloud oxidation of $SO_2$ by $O_3$ and $H_2O_2$: Cloud chamber measurements and modeling of particle growth

Peter Caffrey,[1] William Hoppel,[1,2] Glendon Frick,[1] Louise Pasternack,[3]
James Fitzgerald,[1] Dean Hegg,[4] Song Gao,[4] Richard Leaitch,[5] Nicole Shantz,[5]
Tom Albrechcinski,[6] and John Ambrusko[6]

**Abstract.** Controlled cloud chamber experiments were conducted to measure particle growth resulting from the oxidation of $SO_2$ by $O_3$ and $H_2O_2$ in cloud droplets formed on sulfuric acid seed aerosol. Clouds were formed in a 590 $m^3$ environmental chamber with total liquid water contents ranging from 0.3-0.6 g $m^{-3}$ and reactant gas concentrations <10 ppbv for $SO_2$ and $H_2O_2$ and <70 ppbv for $O_3$. Aerosol growth was measured by comparison of differential mobility analyzer size distributions before and after each 3-4 min cloud cycle. Predictions of aerosol growth were then made with a full microphysical cloud model used to simulate each individual experimental cloud cycle. Model results of the $H_2O_2$ oxidation experiments best fit the experimental data using the third-order rate constant of *Maass et al.* [1999] ($k = 9.1 \times 10^7$ $M^{-2}$ $s^{-1}$), with relative aerosol growth agreeing within 3% of measured values, while the rate of *Hoffmann and Calvert* [1985] produced agreement within 4-9%, and the rate of *Martin and Damschen* [1981] only within 13-18%. Simulation results of aerosol growth during the $O_3$ oxidation experiments were 60-80% less than the measured values, confirming previous results [*Hoppel et al.*, 1994b]. Experimental results and analyses presented here show that the $SO_2$ - $O_3$ rate constants would have to be more than 5 times larger than currently accepted values to explain the measured growth. However, unmeasured $NH_3$ contamination present in trace amounts (<0.2 ppb) could explain the disagreement, but this is speculative and the source of this discrepancy is still unknown.

## 1. Introduction

Cloud processing has been shown to be one of the most important mechanisms for determining the shape of the submicron aerosol size distribution [*Hoppel et al.*, 1986; *Hoppel et al.*, 1994a], increasing the mass of submicron particles in the atmosphere [*Hegg et al.*, 1980; *Hoppel et al.*, 1994a] and moving particles which are too small to be optically important into a size range which can scatter visible light [*Hoppel and Frick*, 1990]. Soluble particles larger than about 0.02 µm in dry radius will activate at cloud supersaturations of less than 1% [*Fitzgerald*, 1973] and grow to cloud droplets sizes of the order of 10 µm in radius, an increase approaching 2 orders of magnitude in radius and an order of $10^6$ in mass. Cloud droplets then scavenge soluble trace gases and oxidants which react in the liquid phase, producing involatile products which remain as increased particulate mass after evaporation of the cloud droplet. Since approximately 90% of clouds which form in the atmosphere reevaporate without precipitating, most of the involatile products formed in cloud droplets get recycled back into the atmosphere as increased aerosol mass when the cloud evaporates.

While cloud processing occurs both over land and oceans, the effect of cloud processing on the size distribution in the marine boundary layer (MBL) is more dramatic than over land, and it is the source of the commonly observed double-peaked feature observed in the submicron size distribution in the MBL. In the MBL the double-peaked features can be related to the average MBL cloud properties in the region [*Hoppel et al.*, 1996], including (1) the size at the minimum between the modes is related to the maximum supersaturation occurring in the MBL clouds, (2) the number of particles under the cloud processed mode is related to the number of cloud droplets, and (3) the ultrafine particles are the cloud interstitial particles which are too small to be activated in the cloud. However, over land the double-peaked feature is not usually evident, presumably a result of numerous distributed aerosol sources filling in the minimum which tends to develop between the two modes. Also, the continental aerosol of a given size is much less homogeneous, consisting of internal and external mixtures of soluble and insoluble components, such that there is not a well defined relationship between size and critical supersaturation of the

---

[1] Remote Sensing Division, Naval Research Laboratory, Washington, D. C.

[2] Now at Computational Physics, Inc., Springfield, Virginia.

[3] Chemistry Division, Naval Research Laboratory, Washington, D.C.

[4] Department of Atmospheric Sciences, University of Washington, Seattle, Washington.

[5] Meteorological Service of Canada, Downsview, Ontario, Canada.

[6] Calspan-University of Buffalo Research Center, Buffalo, New York.

Paper number 2000JD900844.
0148-0227/01/2000JD900844$09.00

particles. Lastly, the boundary layer dynamics which are responsible for the formation of boundary layer clouds are usually less uniform over land than over the ocean.

The process believed to be most important in producing aerosol mass during cloud processing is the oxidation of $SO_2$ by $H_2O_2$ and $O_3$ after dissolution of these trace gases in cloud droplets. The rate constants for oxidation of $SO_2$ by $H_2O_2$ and $O_3$ have been determined from laboratory measurements in bulk samples. Generally, the $O_3$ reaction rate is greater at higher pH (pH >~5), but slows with decreasing pH, and the $H_2O_2$ reaction rate, which is pH independent at pH > 2, is greater at lower pH values. Actual rate measurements in natural clouds or laboratory clouds are difficult to make and nearly nonexistent. There is a concern that the bulk rate constants may not accurately describe the dispersed state where the surface-to-volume ratio of the liquid water is much larger [*Hansen et al.*, 1991; *Jayne et al.*, 1990]. Also, there are gas-phase and liquid-phase transport limitations which must be accounted for in the dispersed state, depending on the speed of the reaction and the size of the droplets.

The Calspan-University of Buffalo Research Center's (CUBRC) 590 $m^3$ environmental chamber is a unique facility with respect to its capability to function as a large expansion cloud chamber. The steel walls are strong enough to withstand the large forces created by pressure differences required for a large chamber to function as an expansion cloud chamber. Since a 10 μm cloud droplet falls at about 0.7 m $min^{-1}$, a large chamber is required if the cloud is to be maintained for the several minutes required to observe the results of the liquid-phase cloud chemistry occurring in the droplets.

Prior measurements at this facility [*Hoppel et al.*, 1994b] demonstrated the high sensitivity of chamber measurements in detecting sulfate formation from oxidation of $SO_2$ by $O_3$ and $H_2O_2$ during cloud processing cycles. These prior measurements indicated that significantly more sulfate was produced by oxidation of $SO_2$ by $O_3$ than predicted by currently accepted rate constants. While large conversion rates were observed with $SO_2$ and $H_2O_2$ present in the chamber, quantitative results were not obtained because there was no in situ measurement of $H_2O_2$.

The objective of the experiments described here was to measure the oxidation rate of $SO_2$ by $O_3$ and $H_2O_2$ in clouds with characteristics similar to natural clouds and compare the rate of sulfate formation with that predicted by the rate constants currently in use. During this deployment to the Calspan chamber, better diagnostic measurements were available than in the previous experiment, including a measurement of gas-phase $H_2O_2$ concentrations.

## 2. Experiment

The experiments were conducted at the Calspan 590 $m^3$ environmental chamber in October and November of 1998. The chamber itself is a 9.1 m diameter, 9.1 m high cylinder with 1.25 cm steel walls coated with a fluoroepoxy type urethane (comparable to FEP Teflon [*Hoppel et al.*, 1994b]), and is capable of overpressurization up to 30 mbar and under-pressurization down to -15 mbar. Full characterization of the physical, operational, and specific experimental characteristics of the chamber was made in May 1998 and are given by *Hoppel et al.* [1999].

### 2.1. Sampling Equipment and Instrumentation

The sampling instrumentation used during these experiments is listed in Table 1. Gas and aerosol samples were taken through several sealed chamber wall ports located ~1.5 m above the chamber floor, while cloud sampling was conducted with instruments placed inside the chamber, all seated approximately 1.2 m above the floor. Chamber concentrations of $SO_2$ were measured with two UV pulsed fluorescence monitors (TECO Model 43s, nominal detection limit (DL) = 0.1 ppb, and the less sensitive TECO Model 43 $SO_2$ (DL = 1 ppb)), and $O_3$ was measured with a UV photometric analyzer (Dasibi 1008-RS $O_3$ monitor, DL = 1.0 ppb). $NH_3$ was monitored with an $NH_3$ to $NO_x$ thermal converter operated at 800°C (Dasibi Model 2109 Thermal Oxidizer, DL ~ 1 ppb), and the $NO_x$ measurement was made with a chemiluminescence analyzer (TECO Model 42, DL = 0.5 ppb). A single sample line for the gas measurements extended 1.3 m into the chamber, containing a 30.5 cm heated borosilicate inlet connected via an Ace-Thread Teflon Swagelock adapter to 4 mm inner diameter PFA Teflon tubing. To remove water as an interferent in the $SO_2$ measurement [*Luke*, 1997], after passing through a stainless steel fitting at the chamber wall the $SO_2$ sample stream was routed through a 61 cm PD-625 Nafion gas drying tube, where it was dried to a relative humidity of <5% by a countercurrent stream of dry sheath air generated from room air drawn through a bed of Drierite. The $NH_3$ and $O_3$ sample lines were each routed to their respective instruments from the chamber wall outlet and did not pass through the Nafion dryer. From the split with the $SO_2$ sample line, the $O_3$ sample stream was routed through approximately 2.1 m PFA tubing to the ozone monitor, and the $NH_3$ stream through 4 m PFA tubing to the $NH_3$ Thermal Oxidizer before passing to the TECO 42 $NO_x$ instrument.

$H_2O_2$ was measured using a tunable diode laser absorption system (TDLAS) designed for tropospheric measurements by

**Table 1.** Sampling Equipment and Instrumentation

| Measurement | Instrument | Detection Limit/Range |
|---|---|---|
| $SO_2$ | TECO 43s | 0.1 ppb |
| | TECO 43 | 1.0 ppb |
| $O_3$ | Dasibi 1008-HV | 1 ppb |
| $H_2O_2$ | Unisearch Assoc. Inc. TDLAS | ~1 ppb |
| $NO_x$ | TECO 42 | 0.5 ppb |
| $NH_3$ | Dasibi 2109 Thermal Converter | 1 ppb |
| Aerosol size distribution | NRL DMA, 44 channels | 6 nm < radius <400 nm |
| Cloud size distribution | PMS CSASP-100-HV | 0.25 μm < radius < 23.5 μm |
| Cloud LWC | Calspan IR | radius < 14 μm |
| CCN | University of Wyoming Model 100a | supersaturation of 0.3%, 0.7% |

Unisearch Associates, Inc. (Model TAMS-150). Samples for the TDLAS system were drawn through ~1.5 m PFA Teflon tubing extending into the chamber, followed by a 2 μm pore-sized Teflon filter and ~5 m additional 4 mm ID PFA Teflon tubing leading the multipass cell for measurement. Measurements were made by alternating background (sample air cleaned through a charcoal filter) and chamber air measurements in 1 min cycles, and typical detection limits were just greater than 1 ppbv [*Hoppel et al.*, 1999].

All aerosol size distribution measurements were made from a dedicated sample line located adjacent to the gas line. Aerosol size distributions were measured with the Naval Research Laboratory Differential Mobility Analyzer (NRL DMA), operated in a scanning mode and measuring the size distribution in 44 channels from 6 nm ≤ radius ≤ 400 nm every 4.5 min. A Met-1 CNC-1100 was used as the particle detector, which has a minimum cutoff size of 0.005 μm. The DMA sheath air was desiccated to relative humidities ranging from 6-20%, and these values (as were all other instrumental measurements) were recorded at a frequency of 1 Hz.

Cloud condensation nuclei (CCN) number concentrations at supersaturations of 0.3% and 0.7% were measured during two experiments with a University of Wyoming Model 100a thermal-gradient diffusion chamber. Total cloud liquid water content (LWC) was measured during all experiments using Calspan's IR Transmissometer System. As described previously [*Hoppel et al.*, 1994b], this IR system uses an 11 μm narrow band pass filter with a 1000°C blackbody source and a folded path length across the bottom of the chamber of 18.3 m. Data reduction followed the methodology of *Chylek* [1978]. Cloud droplet radii were measured with a Particle Measurement Systems Optical Particle Counter (PMS-OPC) classical scattering aerosol spectrometer probe (CSASP) Model 100-HV. The total cloud droplet surface area, volume (LWC), and effective radius were monitored using a Gerber Particulate Volume Monitor (PVM) Model 100A. The IR system is considered to be the most accurate of the two for measuring cloud LWC, as it operates upon the principle of long path absorption and provides an integral signal across the diameter of the lower chamber. The PMS-OPC instrument optically measures individual droplet sizes, and when the droplet number concentration was <350-400 $cm^{-3}$ (equivalent to a counting activity <40%), the PMS-OPC LWC showed good agreement with the other systems. At higher concentrations, however, errors induced by coincidence counting in the PMS-OPC become significant. An empirical correction for these errors obtained from the manufacturer produced good agreement in the total cloud droplet number concentrations with the other instruments, but not with the size distribution (see details in the results sections below). The LWC calculated from these corrected size distributions are typically >1.5 times greater than the IR and PVM systems, suggesting that the existing correction is not reliable for measuring the size distribution. The Gerber PVM generally showed good agreement with the IR system, although with an inherently noisier signal. Comparisons between the IR and PVM instruments are presented in the experimental results.

### 2.2. Experimental Procedure

Prior to each experiment and after the chamber contents were flushed with outside air, the chamber was sealed and then filtered overnight for a minimum of 10 hours through a system consisting of a copper finned dehumidifier, a bank of HEPA filters for particulate removal, and a series of charcoal filters to remove various trace gases (most effectively aromatics and higher molecular weight organic compounds). Particle concentrations were reduced to <0.1 $cm^{-3}$ and $SO_2$ and $O_3$ concentrations to sub-ppb levels, below the detection limits of the instruments.

Prior experiments and characterization measurements made at the chamber [*Hoppel et al.*, 1999] were not able to measure $NH_3$ background concentration levels in the "clean" chamber. During the first week of deployment (out of a total of six), a set of phosphoric acid treated filters were added to the filtration system for $NH_3$ removal, although their efficiency was untested. A set of iodized activated charcoal filters were installed after the first half of the deployment for more complete removal of $NH_3$, and subsequent measurements with the Dasibi 2109 thermal $NH_3$ system showed a gradual reduction to sub-ppb levels during overnight filtering.

Chamber clouds were formed upon sulfuric acid seed nuclei generated from gas phase $SO_2$ oxidation reactions and grown through subsequent condensation to dry sizes of 0.01-0.02 μm. After the overnight filtering, the chamber background levels were monitored for approximately 1 hour, followed by initiation of sulfuric acid aerosol nucleation experiments. The sulfuric acid nuclei were generated in one of two ways, after injection of $SO_2$ (g) to the chamber: (1) formaldehyde ($CH_2O$) was added to the chamber and the chamber photolysis lamps were turned on, after which OH (produced by photolysis of $CH_2O$) oxidized $SO_2$ to sulfuric acid; or (2), $O_3$ was added to the chamber, which reacted with background hydrocarbons to form OH and/or Criegee intermediates, oxidizing $SO_2$ (g) to sulfuric acid. Figure 1a depicts typical growth of the freshly nucleated particles over a 1.5 hour period in preparation for cloud formation.

After growth of the seed nuclei to the desired size ($r \approx 0.01$-$0.02$ μm, dry size), the particle concentration was reduced to

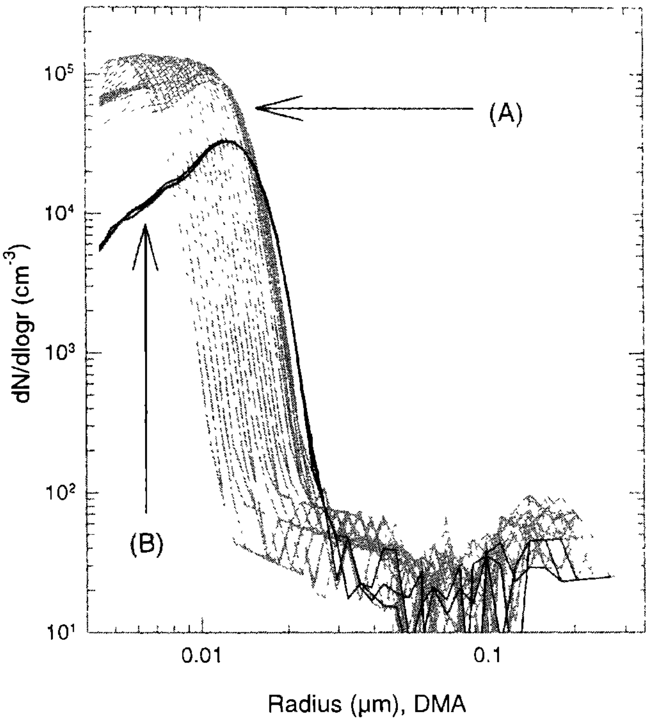

**Figure 1.** (curve a) Growth of a typical cloud-processing seed aerosol, with DMA measured size distributions plotted at 4.5 min intervals measured prior to run D. Aerosol growth is a result of condensation of $H_2SO_4$ produced from gas phase $SO_2$ - $O_3$ reactions. (curve b) Cloud-processing seed aerosol prior to cloud formation, after filtration to reduce CCN concentrations.

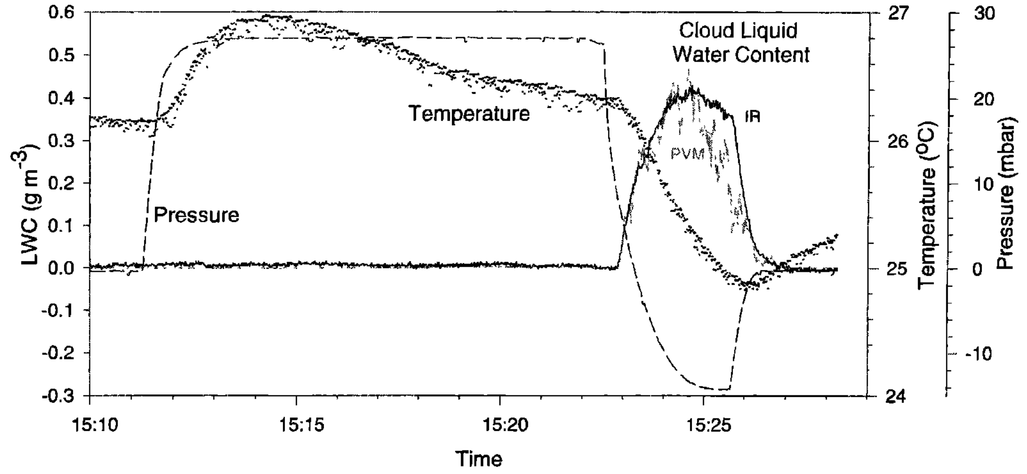

**Figure 2.** Cloud and cloud chamber measurements during a typical cloud formation cycle, from run D (November 4, 1998), with the dashed line representing the chamber pressure, the wide dotted line showing the chamber temperature, and the cloud liquid water content represented by two overlapping lines for the IR instrument (solid line) and the PVM instrument (greyed line).

levels appropriate for cloud formation by filtering the chamber contents through the chamber's HEPA filters. A typical precloud, postfiltering aerosol size distribution is shown in Figure 1b. The chamber atmosphere was then humidified by injection of ~ 42 L of deionized water through a ring located at the top circumference of the chamber, with the water running down the walls and collecting on the floor of the chamber in several small pools. The relative humidity (RH) was monitored with chilled-mirror dew point sensors at two locations. After the chamber RH approached 100%, the chamber contents were compressed to 25-30 mbar above atmospheric pressure with filtered outside air. The RH was allowed to reequilibrate after the compression back to near saturated conditions (typically ~10 min), during which time reactant ($SO_2$, $O_3$ or $H_2O_2$) concentrations were adjusted to the desired experimental levels.

Reactant levels of $SO_2$, $O_3$, and $H_2O_2$ were controlled by gas phase injections through ~1 m PFA teflon tubing from sealed chamber ports located midway up the chamber wall. The chamber contents were kept well mixed before and after cloud formation by an in-chamber mixing fan. $SO_2$ was added from a 0.5% $SO_2$ (in $N_2$) Scott Specialty Gas cylinder, and concentrations were monitored with the TECO $SO_2$ instrumentation to achieve desired reactant levels. $O_3$ was added from the output of a Welsbach Laboratory Ozonator, which formed ozone from high purity oxygen passing over a high voltage electrode. $H_2O_2$ was injected by passing research grade $N_2$, acting as a carrier gas, over a bath of 50% $H_2O_2$ heated to approximately 50°C. The subsequent $H_2O_2$ - $N_2$ mixture was diluted with a second flow of $N_2$ to prevent line condensation before introduction to the chamber. Injection rates into a wet chamber measured during a May, 1998 characterization study ranged from 0.23-0.29 ppbv $min^{-1}$ [*Hoppel et al.*, 1999]. $H_2O_2$ concentrations were monitored in real time with the TDLAS system.

Figure 2 contains measurements of the chamber pressure, temperature, and cloud LWC during a typical cloud cycle (measurements from November 4, cloud 1), including the initial compression. After chamber equilibration during overpressurization, clouds were formed by the rapid expansion of the chamber contents by venting the over-pressurized chamber air to background levels, and then to -15 mbar (below atmospheric pressure) by venting through a forced air blower.

The cloud formation (cloud LWC) was monitored in real time via the PVM instrument. Activation of the CCN and formation of the cloud typically began ~15-30 s after the pressure expansion was initiated (equivalent to a pressure expansion of ~15-20 mbar), as seen in Figure 2. The total cloud LWC then increased to a maximum value of 0.4-0.5 g $m^{-3}$ before beginning to slowly decrease until cloud dissipation at the end of the cycle. At the conclusion of an experiment the cloud was quickly evaporated by venting in filtered outside air to bring the chamber pressure back to atmospheric levels.

The slow decrease in cloud LWC from a maximum value achieved near the maximum expansion (minimum in chamber pressure) was consistently measured in each cloud formation experiment ($n$>50), and is presumed to result from heat loss from the enclosed area surrounding the chamber through the uninsulated chamber walls into the chamber itself. As a result, the cloud droplets, after growing to a maximum size, began to slowly evaporate.

To assess changes in the aerosol size distribution from the cloud processing, the initial size distribution was measured immediately before the compression of the chamber, or approximately 15 min before cloud formation. Aerosol growth was measured by comparison of several DMA size distributions measured immediately after cloud dissipation to the initial, precloud distribution. Given the size of the cloud droplets formed ($R$<15 μm) and the duration of the clouds (2-4 min), changes to the aerosol size distribution by cloud droplet coalescence are negligible, and all SD changes are attributed to the addition of sulfate mass from the aqueous phase oxidation of $SO_2$.

## 3. Cloud Modeling

A computer model was developed to assess the results of the experimental measurements, including simulation of cloud formation and evolution during the chamber pressure expansion, in-cloud oxidation of specified levels of $SO_2$ by $O_3$ and $H_2O_2$, and changes to the original aerosol size distribution as a result of mass added from the aqueous-phase reaction products.

Details of the model are given below, and comparison of model results with the experimental measurements for $SO_2$ oxidation by $H_2O_2$ and $O_3$ follow in the final two sections.

### 3.1. Cloud Microphysics

Cloud formation in the chamber was simulated using an adiabatic cloud parcel model, computing the evolution of a discrete population of nuclei/droplets as a result of cooling due to an expansion of the air parcel. The initial nuclei population was input from DMA measurements of the aerosol size distribution before cloud formation (and before the chamber over-pressurization, as discussed above), and the input aerosol particles were assumed to be composed of sulfuric acid in equilibrium with water vapor at the measurement humidity. The expansion rate was determined from the measured chamber pressure during the cloud cycle, and these data were input directly to the model at a frequency of 1 Hz.

The model computations begin at a relative humidity of 100%. Although during the experiments the chamber air was allowed to equilibrate with the water injected for humidification, typically the first 10 to 15 mbar of the expansion was needed to reach saturation and for cloud formation to begin. Thus the saturation point in the modeling was taken to be the time at which liquid water was first detected by the IR transmissometer, adjusted when necessary to produce model cloud formation at the same time in the pressure expansion as that which was measured.The change in chamber temperature due to adiabatic expansion (for a given $dP$) is calculated as

$$\frac{dT}{T} = \frac{R_g}{M_a C_p}\frac{dP}{P} + \frac{L_{ew}}{C_p T \rho_a} dM , \tag{1}$$

where $T$ is temperature, $R_g$ is the universal gas constant, $M_a$ and $C_p$ are the molecular weight and specific heat of air, $P$ is chamber pressure, $L_{ew}$ is the latent heat of condensation of water, $\rho_a$ is the density of air, and $dM$ is the change in mass of condensed liquid water per unit volume of air (change in LWC) due to cloud droplet growth/dissipation. The temperature change is calculated at time steps of 0.01 s, with the expansion assumed to change linearly between each input pressure value.

As discussed in the experiment section, the decrease in the measured cloud LWC while the cloud was held at minimum pressure (see Figure 2) is presumed to be a consequence of heat transfer through the chamber walls, thus rendering the chamber nonadiabatic. A correction to equation (1) for departure from adiabatic conditions was accomplished by reducing the calculated temperature during each time step by a constant amount empirically determined to match the predicted LWC versus time to the measurements made for each run. These corrections ranged from 0.12-0.21°C $min^{-1}$ for runs presented here.

Chamber supersaturation $S$ is determined at each temperature (time step) as

$$S_t = \frac{\left[ e_{t-1}\dfrac{P_t}{P_{t-1}} + \dfrac{R_g T_t}{M_w} dM \right] - e_{sat,t}}{e_{sat,t}} \tag{2}$$

which explicitly calculates $S$ at each time step $t$ as the change in water vapor pressure due to expansion and condensation as compared to the temperature-dependent saturation vapor pressure $e_{sat}$. The saturation vapor pressure is calculated using the temperature dependence of *Lowe and Ficke* [1974].

Associated with each bin of the DMA is a critical supersaturation, and as the computed chamber supersaturation rises due to the pressure expansion, DMA bins are successively activated to cloud droplets as the supersaturation exceeds the critical supersaturation of each bin. When a bin is activated, the number concentration of particles in that bin are introduced as growing droplets at the critical activation radius associated with that bin. The critical supersaturation $S_c$ and the critical radius $r_c$ are determined from *Pruppacher and Klett* [1997] as

$$S_{c,i} = \sqrt{\frac{4A^3}{27B_i}} \tag{3}$$

$$r_{c,i} = \sqrt{3B_i / A} , \tag{4}$$

where

$$A = \frac{2 M_w \gamma_w}{R_g T \rho_w} \tag{5}$$

$$B_i = \frac{M_w \sum n_{j,i} \phi_{j,i}}{\frac{4}{3}\pi \rho_w} \tag{6}$$

and $\gamma_w$, $\rho_w$, and $M_w$ are the surface tension, density, and molecular weight of water, and $n_{j,i}$ and $\phi_{j,i}$ are the number of moles and the osmotic coefficient of the $j^{th}$ ion in the $i^{th}$ droplet size, respectively. We note that $A$ and $B$ are the terms that describe the Kelvin and colligative effects on vapor pressure, where $\exp(A/R_i)$ describes the effect of particle curvature (Kelvin effect), and $\exp(-B_i/R_i^3)$ describes solute effects (colligative effects). Also, the weak solution approximation of $\phi_{j,i} = 1$ was used in all modeling runs.

Initially, and to determine the critical supersaturation $S_{c,i}$, $B_i$ is calculated for each particle size using the sum of 3 times the number of moles of sulfuric acid. This assumes complete dissociation of each sulfuric acid molecule to 2 $H^+$ and 1 $SO_4^{2-}$ molecules. The number of moles of sulfuric acid is calculated from the dry particle volume (0% RH), where the dry particle radius is calculated from the radius measured at the DMA humidity using the $H_2SO_4$ activity data of *Giauque et al.* [1960] and density data from *Lide* [1990] using no corrections for particle curvature (see *Hoppel et al.* [1996] for description).

As the aerosol size distribution is input directly from DMA measurements, particle sizes are represented in the model as the midpoint of each DMA bin, calculated as the geometric mean of the bin boundaries. Cloud droplet growth is modeled by allowing the midpoints to grow and shrink, with the particle number concentration in each bin therefore remaining constant.

The initial size distribution was typically very steep (see Figure 1), with large changes in concentration over a small range of particle radii and large particle concentrations in each DMA size bin. Since the particle sizes input to the model are determined by the DMA bin size intervals, often only a fraction of the particles in the last channel activated by the model are necessary to match the CCN number concentrations measured in the chamber experiment. Resolving the measured aerosol size distribution into a greater number of channels would allow for activation of only those particles in the bin that are larger than the critical radius. Thus, when necessary to produce agreement with the measurements, the particle concentration in the last activated bin in the input size distribution was adjusted to reflect the measured cloud droplet number concentration.

Droplet growth in each activated DMA bin $i$ is then calculated from

$$\frac{dR}{dt} = \frac{G_i}{R_i}\left[S - \frac{A}{R_i} - \frac{B}{R_i^3}\right], \tag{7}$$

where $G_i$ is calculated as

$$G_i = \left(\frac{\rho_w R_g T}{e_{sat} D^*_{v,i} M_w} + \frac{L_{ew}\rho_w}{k^*_{a,i} T_\infty}\left[\frac{L_{ew} M_w}{T R_g} - 1\right]\right)^{-1} \tag{8}$$

$D_v^*$ and $k_a^*$ are the diffusivity for water vapor and thermal conductivity of humid air, respectively, each corrected for gas kinetic effects and determined using the temperature dependence as outlined in *Pruppacher and Klett* [1997] and *Fitzgerald* [1972] as

$$D^*_{v,i} = \frac{D_v}{\left[\frac{R_i}{R_i + \lambda_a} + \frac{D_v}{R_i \alpha_c}\left(\frac{2\pi M_w}{R_g T}\right)^{1/2}\right]} \tag{9}$$

$$k^*_{a,i} = \frac{k_a}{\left[\frac{R_i}{R_i + \lambda_a} + \frac{k_a}{R_i \alpha_T \rho_a c_p}\left(\frac{2\pi M_a}{R_g T}\right)^{1/2}\right]}. \tag{10}$$

Here the thermal accommodation coefficient ($\alpha_T$) = 1.0, the vapor accommodation coefficient ($\alpha_T$) = 0.5, and $\lambda$ was calculated as a function of temperature and pressure [*Hinds*, 1982] as

$$\lambda = \left(\frac{\sqrt{2}\pi P N_a}{R_g T} dm_a\right)^{-1}, \tag{11}$$

where the $dm_a$, the collision diameter for air, was 3.7 x $10^{-8}$ cm and $N_a$ is Avogadro's number.

Simulation of cloud formation was generally very good, with both the measured LWC and peak cloud droplet size closely matching the measurements. Details of model performance are given in the discussion of the experimental and modeling results that follow.

### 3.2. Cloud Chemistry

The aqueous phase chemistry in the model is initialized with the specification of the measured partial pressures of $SO_2$, $O_3$, $H_2O_2$, and $NH_3$. Carbon dioxide ($CO_2$) is also included in all runs at an assumed background level of 350 ppm. Gas-aqueous phase dissolution and aqueous phase dissociation reactions and corresponding rate constants that are included in the model are listed in Table 2. Each equilibrium constant was correct to the initial chamber temperature by

$$K_T = K_{298}\exp\left(\frac{\Delta H_{298}}{R_g}\left[\frac{1}{298} - \frac{1}{T}\right]\right), \tag{12}$$

where $K$ is the equilibrium constant at temperature $T$, and $\Delta H$ is the reaction enthalpy at 298 K.

Prior to the pressure expansion, and then after each cloud droplet growth time step, the newly sized droplets were re-equilibrated with the gas phase components, conversion of $SO_2$ was calculated via the appropriate aqueous phase reaction, and the droplet and gas phase concentrations were re-equilibrated based upon the new [S(VI)] and pH. The model equilibrates the gas and aqueous (cloud droplet) phase components by solving the charge conservation equation in each size bin $i$ as

$$\begin{aligned}[H^+]_i + [NH_4^+]_i = [OH^-]_i + [HSO_3^-]_i + 2\,[SO_3^{2-}]_i \\ + 2\,[SO_4^{2-}]_i + [HSO_4^-]_i + [HCO_3^-]_i + 2\,[CO_3^{2-}]_i\,,\end{aligned} \tag{13}$$

where the aqueous phase concentrations are kept at Henry's law equilibrium.

At the start of the modeling, the sizes of the sulfuric acid particles are adjusted to their sizes at RH = 100%. The input gas concentrations are assumed to be in equilibrium with the particle phase, and therefore aqueous phase concentrations are added to the wet aerosol to achieve this equilibrium. The "total"

**Table 2.** Equilibrium Constants

| Reaction | K | | $\Delta H_{298}$, |
|---|---|---|---|
| | Value | Units | kcal $mol^{-1}$ |
| $SO_2$ (g) ↔ $SO_2$(aq) = $SO_2 \cdot H_2O$ (aq) | 1.2 | $M$ $atm^{-1}$ | -6.25 |
| $SO_2 \cdot H_2O$ (aq) ↔ $HSO_3^-$ (aq) + $H^+$(aq) | 0.0129 | $M$ | -4.16 |
| $HSO_3^-$ (aq) ↔ $SO_3^{2-}$ (aq) + $H^+$ (aq) | 6.014 x $10^{-8}$ | $M$ | -2.23 |
| $O_3$(g) ↔ $O_3$(aq) | 0.011 | $M$ $atm^{-1}$ | -5.04 |
| $H_2O_2$(g) ↔ $H_2O_2$ (aq) | 7.4 x $10^5$ | $M$ $atm^{-1}$ | -14.5 |
| $NH_3$ (g) ↔ $NH_3$ (aq) | 74 | $M$ | -8.17 |
| $NH_3$ (aq) + $H_2O$ ↔ $NH_4^+$ (aq) + $OH^-$ (aq) | 1.7 x $10^{-5}$ | $M$ | 0.9 |
| $HSO_4^-$ (aq) ↔ $SO_4^{2-}$ (aq) + $H^+$ (aq) | 0.012 | $M$ | - |
| $CO_2$ (g) ↔ $CO_2$(aq) = $CO_2 \cdot H_2O$ (aq) | 0.034 | $M$ $atm^{-1}$ | -4.85 |
| $CO_2 \cdot H_2O$ (aq) ↔ $HCO_3^-$ (aq) + $H^+$(aq) | 4.3 x $10^{-7}$ | $M$ | 1.83 |
| $HCO_3^-$ (aq) ↔ $CO_3^{2-}$ (aq) + $H^+$ (aq) | 4.68 x $10^{-11}$ | $M$ | 3.55 |

**Table 3.** Cloud Model Kinetic Expressions, Constants

| Oxidant | Rate Expression | | Rate Constants, $M^{-2}\,s^{-1}$ | Reference |
|---|---|---|---|---|
| $O_3$ | $\left(k_0[SO_2]+k_1[HSO_3^{1-}]+k_2[SO_3^{2-}]\right)\times[O_3]$ | (3-1) | $k_0$ 2.4 x $10^4$<br>$k_1$ 3.7 x $10^5$<br>$k_2$ 1.5 x $10^9$ | *Hoffman and Calvert* [1985] |
| $H_2O_2$ | $k\ [H^+][H_2O_2][HSO_3^-]$ | (3-2) | 9.1 x $10^7$ | *Maass et al.* [1999] |
| $H_2O_2$ | $\left[\frac{k}{1+13[H^+]}\right][H^+][H_2O_2][HSO_3^-]$ | (3-3) | 7.45 x $10^7$ | *Hoffman and Calvert* [1985] |
| $H_2O_2$ | $\left[\frac{k}{[H^+]+0.1}\right][H^+][H_2O_2][HSO_3^-]$ | (3-4) | 5.2 x $10^6$ | *Martin and Damschen* [1981] |

concentration of a species, i.e., the gas and aqueous phase combined, is then calculated and adjusted at each timestep for loss (consumption: $SO_2$, $O_3$, $H_2O_2$) or gain (S(VI)) by the $O_3$ or $H_2O_2$ aqueous phase oxidation reactions.

For the aqueous phase reactions, kinetics of the $SO_2$ - $O_3$ (aq) reaction were taken from *Seinfeld and Pandis* [1998] as reported from *Hoffmann and Calvert* [1985], and the rate expression and rate constants used here are listed in Table 3 (equation (3-1)). Unlike this expression, more recent data described by *Botha et al.* [1994] have supported a rate expression with a dependence on $[H^+]^{1/2}$. Evaluation of this rate mechanism at pH values ranging from 1 to 7 shows the effective rate constant to be lower than that for the Hoffmann expression. As the Hoffmann expression was derived based upon an evaluation of several sets of experimental results, we have chosen to present only the results of modeling using the Hoffmann formulation.

A review of $H_2O_2$ - $SO_2$ aqueous phase oxidation kinetics from recent modeling studies has shown that two rate constants are typically employed. Models by Bower et al. [*Bradbury et al.*, 1999; *Bower et al.*, 1999; *Wells et al.*, 1998; *Bower et al.*, 1997; *Bower et al.*, 1991], *Sander and Crutzen* [1996], *Liu and Seidl* [1998], and *Tremblay and Leighton* [1986] employ the form reported by *Martin and Damschen* [1981], listed in Table 3 as equation (3-4). Others [*O'Dowd et al.*, 1999] use the form from *Hoffmann and Calvert* [1985], taken as a best fit through a composite of independent measurements (equation (3-3) in Table 3).

A new study by *Maass et al.* [1999] reports measurements of the third-order $H_2O_2$ - $SO_2$ rate constant at reactant concentrations typical of cloud droplets of 9.1( ± 0.5) x $10^7$ $M^{-2}$ $s^{-1}$ (equation (3-2) in Table 3), or 1.2 times that of *Hoffmann and Calvert* [1985] and 1.75 times that of *Martin and Damschen* [1981]. The *Maass et al.* [1999] value is valid for ionic strength solutions $I_c$ of ≤1.5 x $10^{-4}$ *M*, and is therefore applicable to the conditions of these experiments; the maximum ionic strength reached in a cloud droplet for a typical experiment conducted here, as predicted by the model, is <7 x $10^{-5}$ *M* (run A, as detailed below). To compare the effectiveness of these three formulations in predicting the measured cloud chamber growth, each has been used in this modeling.

### 3.3. Mass Transport Limitations

Following the methodology of *Schwartz* [1988], it was determined that mass transport limitations are significant in the $SO_2$ - $O_3$ system for aqueous phase diffusion of $O_3$ at droplet pH >~4.5, and in the $SO_2$ - $H_2O_2$ system for aqueous phase diffusion of $H_2O_2$ at pH<~3.5. These values were determined using reactant levels and cloud droplet sizes appropriate for these experiments (see Tables 4 and 6 for details). Therefore corrections to the $SO_2$ - $O_3$ reaction rate due to $O_3$ mass transfer effects in both the gas and aqueous phases were included in the modeling by reducing $[O_3]$ from the Henry's law equilibrium value (considered valid only at the surface of the droplet) to an average droplet concentration as [*Schwartz*, 1988]

$$[O_3]_{avg} = \frac{Q_{aq}}{Q_g}\times[O_3]_{surface} \tag{14}$$

$$Q_{aq} = 3\left[\frac{\coth q}{q}+\frac{1}{q^2}\right] \tag{15}$$

**Table 4.** Experimental Results, $SO_2$ - $H_2O_2$ Cloud Processing

| Run | Date | $SO_2$, ppb | $H_2O_2$, ppb | CCN, $cm^{-3}$ DMA[a] | PMS | CCN | Max LWC, $g\,m^{-3}$ | Aerosol Radius, r μm Initial[b] | Final | Cloud Radius, R, μm | r/R | Cloud Duration,[c] s | Aerosol ΔVol, $\mu m^3\,cm^{-3}$ |
|---|---|---|---|---|---|---|---|---|---|---|---|---|---|
| A | Nov. 5 | 1.2 | 4.7±0.22 | 240/310 | 250 | na[d] | 0.46 | 0.0156 | 0.095 | 7.5 | 0.0126 | 150 | 0.904 |
| B | Oct. 14 | 2.0 | 2.1±0.08 | 360/530 | 475 | 386 (0.3%)<br>468 (0.7%) | 0.47 | 0.0164 | 0.090 | 6.1[e] | 0.0146 | 185 | 1.011 |
| C | Nov. | 1.8 | 7.4±1.4 | 490/550 | 550 | na | 0.60 | 0.0143 | 0.076 | 6.4[e] | 0.0118 | 140 | 0.998 |

[a] Aerosol number concentration in cloud-processed peaks, listed as (peak 1/ peak 1 + peak 2).
[b] Minimum CCN radius.
[c] Time from cloud formation till pressure equalization.
[d] na, not available.
[e] R is radius of droplet of average volume at time of maximum LWC.

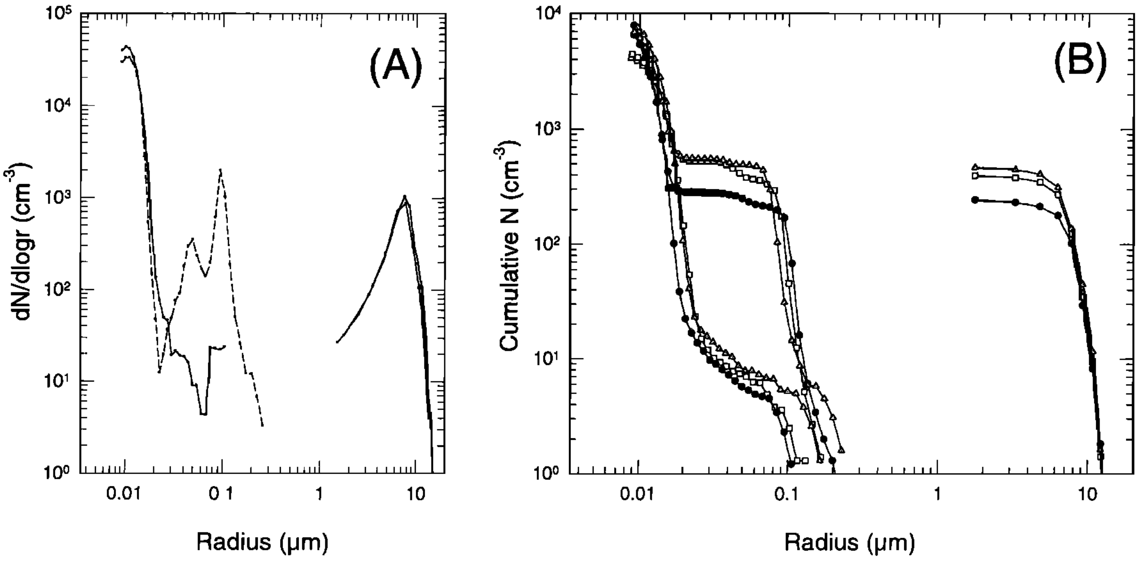

**Figure 3.** (a) Measured aerosol growth from in-cloud conversion via $SO_2$ - $H_2O_2$ (aq) reactions for run A, with the solid line on the left the initial size distribution (SD), the dashed the postcloud SD, and two solid lines on the right the corresponding cloud droplet SD, all as dN dlogr$^{-1}$ (cm$^{-3}$) versus dry radius (aerosol) and wet radius (cloud), in μm. (b) Cumulative aerosol and cloud droplet SDs for runs A-C.

$$Q_g = 1 + \frac{R_g T Q_{aq} k' R^2}{3 D_v^*} \qquad (16)$$

$$q = R_{drop} \left( \frac{k'}{D_{aq}} \right)^{\frac{1}{2}}, \qquad (17)$$

where $D_{aq}$ ($O_3$) = 1.8 x $10^{-5}$ cm$^2$ s$^{-1}$, $D_g$ ($O_3$) = 0.126 cm$^2$ s$^{-1}$, $k'$ = effective first-order rate constant for the $SO_2$ - $O_3$ reaction, $R$ = cloud droplet radius, and $R_g$ is the universal gas constant.

No corrections were included for $H_2O_2$ mass transfer limitations, as the initial radii of CCN during all these experiments were < 0.02 μm, and activating 0.02 μm particles to the smallest peak cloud droplet size (6 μm) yields an initial droplet pH of ~5.9. Using a minimum cloud droplet size of 6 μm, a droplet pH of ≤3.5 would be reached only when the residual sulfuric acid particle radius ≥0.123 μm. The largest peak dry aerosol radius measured during this experiment was 0.094 μm, and <2% of the CCN were at sizes >0.12 μm in the largest postcloud processing dry aerosol size distribution for any of the runs (details are in results section). Therefore $H_2O_2$ mass transfer limitations were negligible for these experiments, and no calculations were included in the modeling.

## 4. Hydrogen Peroxide Results

### 4.1. Chamber Measurements

Aerosol growth via the $SO_2$ (aq) - $H_2O_2$ (aq) reaction was measured during three experiments conducted on November 5, October 14, and November16, 1998 (hereafter runs A, B, and C). A summary of the reactant concentrations and results for each are listed in Table 4. The results from run A are displayed in Figure 3a, showing the precloud and postcloud dry aerosol size distribution and the PMS-OPC measured cloud droplet distributions measured at the time of maximum cloud LWC. The dry aerosol sizes were calculated assuming a particle composition of sulfuric acid. Figure 3b displays the cumulative size distributions for all three runs. As can be seen there, in each run seed aerosol from larger than 0.014 μm (dry radius) were activated to form cloud droplets with a peak radii ranging from 6-8 μm. Subsequent peak channel (dry) growth from accumulation of sulfuric acid was over 5 times the initial size, growing to $r$ = 0.075-0.095 μm, an increase in volume of approximately 125 times. The reactant gas phase concentrations varied from 1.2 to 2.0 ppb for $SO_2$ and from 2.1 to 7.7 ppb for $H_2O_2$.

Increases in the aerosol volume concentration were remarkably consistent between the three separate experiments, ranging from 0.90 to 1.01 μm$^3$ cm$^{-3}$ (see Table 4). Each run also produced aerosol growth in two modes, with a larger, primary mode located at $r_{dry}$>0.07 μm, and a secondary, smaller (by varying degrees) mode at $r_{dry}$ from 0.02-0.04 μm. The larger mode accounts for nearly all the mass increase. CCN concentrations, measured as the cumulative number concentration in the cloud processed peaks, ranged from 310 to 550 cm$^{-3}$, and run B exhibited the largest secondary peak. Additionally, measurements of CCN were made at nominal supersaturations of 0.3% and 0.7% after cloud dissipation on October 14 (run B), and measured concentrations of 386 ± 60 cm$^{-3}$ and 468 ± 70 cm$^{-3}$, respectively, are in good agreement with the number of particles under the cloud processed mode (CCN measurements were not made during runs A and C). Model results presented in the next section predict peak cloud supersaturations of 0.85% for this run, greater than the CCN measurement value of 0.7%. Comparison of the cloud droplet concentrations with the cloud processed DMA concentrations is shown in the cumulative size distributions in Figure 3b, where PMS distributions taken near the point of maximum LWC are shown.

As detailed in the experimental discussion, >~ 350-400 cm$^{-3}$ cloud droplets produced significant coincidence counting errors in the PMS-OPC instrument. The manufacturer supplied correction for coincident counting gave a fairly reliable

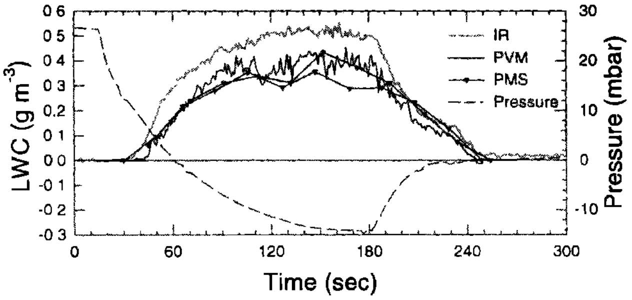

**Figure 4.** Pressure expansion and measured cloud liquid water content, run A.

correction for number concentration, but not for the size distribution. This resulted in unreliable measurements of the cloud droplet distribution and PMS-OPC determined LWC for clouds formed during runs B and C. Therefore cloud radii values listed in Table 4 for runs B and C are the radius of a droplet of average volume, calculated from the peak LWC and the activated number concentration measured by the DMA.

Examining the results of run A shows the DMA-measured CCN number concentration in the primary peak (240 cm$^{-3}$) in excellent agreement with the PMS-measured cloud droplet number concentration (250 cm$^{-3}$). The LWC (IR, PVM, and PMS) and pressure measurements made during the cloud formation process for run A are displayed in Figure 4. Unique to this experiment (run A), there is significant disagreement between the IR LWC measurement and the PVM and PMS measurements, while the PVM and PMS measurements are in good agreement. Measurements of a second cloud formed on this day show a similar discrepancy, but all other experiments showed good agreement between the IR and PVM systems. The source of the discrepancy measured on this day is unknown. Malfunction of the PVM seems unlikely, and the PMS-OPC measured number concentration was below the instrument's saturation threshold. The agreement between the PMS and PVM measurements suggest that either 1) the IR readings are erroneous or 2) the conditions at the in-chamber sampling location of the PMS/PVM instruments was different enough from the rest of the chamber to delay the activation point during the expansion and a produce a lower LWC (smaller droplet size). However, this second effect was not measured on any of the other days when experiments were conducted. It is suspected that during run A, the IR beam was slightly out of alignment, as the IR baseline did shift from its pre-cloud value upon cloud dissipation, an effect which would become more pronounced as the chamber walls moved slightly during the pressure expansion. Therefore the IR-LWC measurement during run A is discounted, and the PVM and PMS measurements for this Run will be used in further analysis.

### 4.2. Modeling Results

Results of the model simulation of cloud formation for run A are shown in Plates 1a and 1b, with Plate 1b comparing individual cloud droplet distributions to the PMS measurements and Plate 1a depicting the model versus measured LWC over the lifetime of the cloud. Good agreement is seen in the model's ability to reproduce the measured total cloud LWC over time, which was typical for all experiments. Also, the modeled droplet distributions are seen to be much narrower than the observed droplet distributions, which are plotted at 20 s intervals in Plate 1b. However, there is good agreement with the location of the peak radius and the LWC. The narrowness of the droplet distribution calculated with an adiabatic (in this case sub-adiabatic) parcel model is well known. Even if the real size distribution in the chamber were as narrow as that predicted by the parcel model, there would be considerable broadening of the measured distribution due only to the resolution of the PMS-OPC [*Baumgardner and Spowart*, 1990; *Dye and Baumgardner*, 1984]. If the droplet distribution were as narrow as predicted by the parcel model, it would be evident in the width of the residual aerosol cloud processed mode. However, the broad peak measured in the cloud droplet size distribution is also measured in the residual aerosol cloud-processed mode, as seen in Figure 3a, and similar agreement was seen in runs B and C. Therefore the observed broadening of the cloud droplet distribution is believed to be largely due to the spatial variation of temperature and humidity in the chamber prior to and during the cloud formation, during which time the mixing fan is turned off (to prevent cloud droplets from impacting out). After cloud dissipation, the mixing fan is turned back on.

Model-predicted aerosol growth for run A is shown in Plate 2b, with the residual aerosol plotted at 30 second intervals, using kinetics of *Hoffmann and Calvert* [1985]. The model-predicted growth for the aerosol and cloud droplet of the smallest activated DMA channel is depicted in Plate 2a. Growth laws outlined previously [*Hoppel et al.*, 1994b] have shown that $r$, the aerosol radius, is directly proportional to the cloud droplet radius $R$ and to the cube root of $P_{SO2}$, $P_{H2O2}$, and $t$ (duration of cloud droplet), shown in equation (18). Since the radius (as opposed to mass) is the more fundamental measurement of the DMA and since any errors in $P_{H2O2}$, $P_{SO2}$, and $t$ enter only as a cube root, it is appropriate to use the measured and calculated ratios of $r$, normalized to the cloud droplet radius as $r/R$, as a unit of comparison.

$$\frac{r}{R} \propto \left(P_{H_2O_2} P_{SO_2} t\right)^{1/3} . \tag{18}$$

Comparisons of the growth predicted using the three different kinetic formulations for runs A and B are listed in Table 5, and the results for run A are displayed in Plate 3. As seen there, the best agreement for each of these experiments is reached using the recently published kinetic data from *Maass et al.* [1999]. The model-predicted aerosol radius using the Maass et al. formulation is 6% and 17% greater than the HC85 and MD81 results, respectively, and 95% and 91% of the measured radius in each case, respectively. More importantly, the normalized growth ($r/R$) for these two runs is 97% and 102%, within 3% of measured, well within the uncertainty of these measurements.

## 5. Ozone Oxidation Results

### 5.1. Chamber Measurements

Table 6 summarizes results of six experiments conducted measuring aerosol growth via the $SO_2$ (aq) - $O_3$ (aq) reaction (hereafter runs D-I). $SO_2$ concentrations in these experiments ranged from 2.0 to 3.5 ppb, $O_3$ concentrations ranged from 60 to 77 ppb, and cloud LWC ranged from 0.42-0.50 g m$^{-3}$. Cloud droplet concentrations were low enough to collect PMS-OPC droplet size spectra only during Runs D and E and the aerosol and cloud droplet size distributions from these two runs are displayed in Figure 5. The cloud droplet distributions displayed there were measured at the time of each cloud's maximum

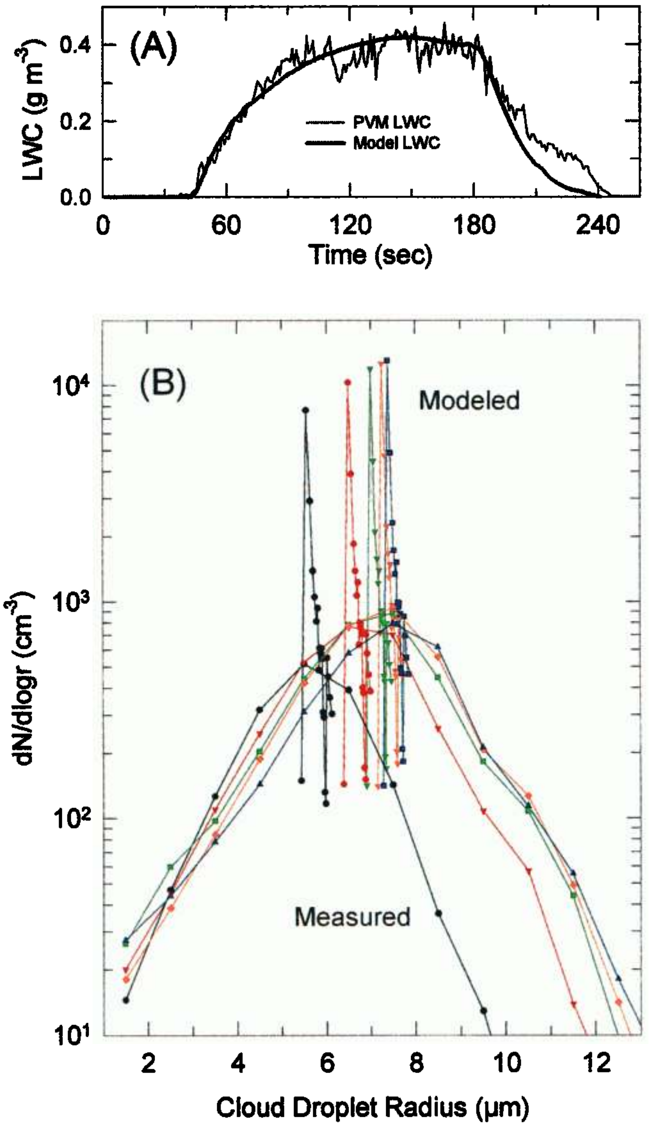

**Plate 1.** Modeling results of cloud formation, run A. (a) Modeled and measured (PVM) cloud LWC, and (b) modeled cloud droplet distributions compared with PMS-OPC measurements at 30 s intervals.

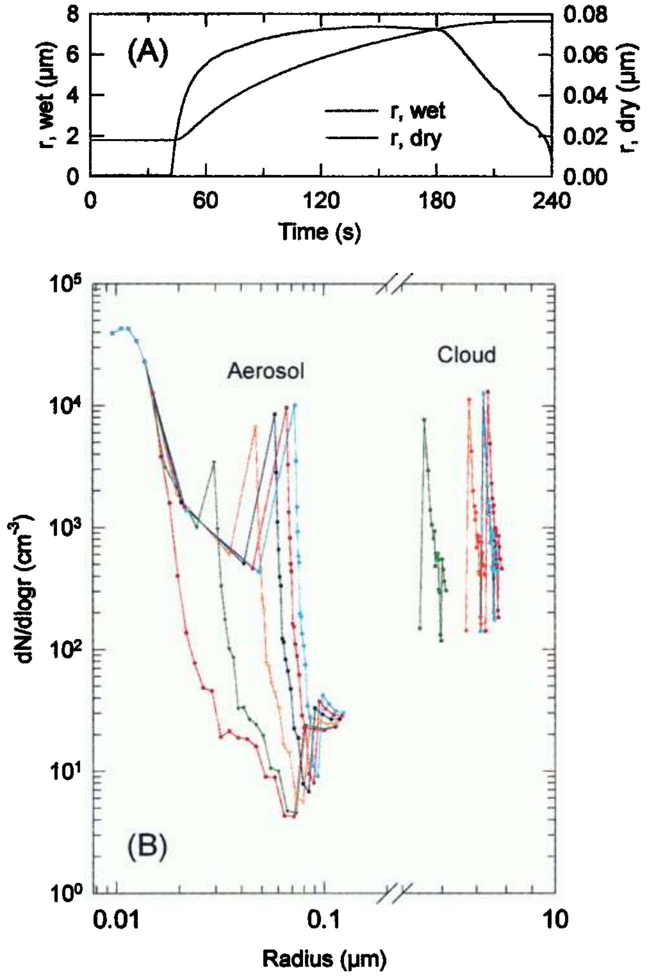

**Plate 2.** Model results, run A, $SO_2$ - $H_2O_2$ conversion. (a) Aerosol and cloud droplet radius during the cloud cycle, shown for the smallest activated size bin, and (b) cloud droplet and residual dry aerosol size distributions at 30 s intervals.

LWC, and the aerosol radii have been corrected to dry sizes as sulfuric acid particles. Figure 2 contains a temporal plot of the chamber pressure and the LWC (as measured by the IR and PVM systems) for run D, where good agreement is seen between the two LWC measurements, as previously discussed. Also of note are the excellent agreement in the number of cloud droplets measured with the PMS-OPC and the number of cloud droplets implied from the cloud processing mode of the DMA size distribution, as listed in Table 6. These are essentially equivalent for each run, with 300 cm$^{-3}$ CCN activated during run D and 400-450 cm$^{-3}$ for run E.

Aqueous phase $SO_2$ oxidation by $O_3$ during each cloud grew the activated particles to a mode at the dry radius sizes of 0.068 μm and 0.045 μm for runs D and E, respectively. The gas phase concentrations for both runs were nearly identical ($SO_2$ = 3 and

**Table 5.** $SO_2$ - $H_2O_2$ Modeling Results[a]

| Run | Date | S, % | Final Aerosol Radius *r* μm | | | | Cloud Droplet *R*, μm | | *r/R* | | | |
|---|---|---|---|---|---|---|---|---|---|---|---|---|
| | | | Measured | MD81 | HC85 | M99 | Model | Measured | Measured | MD81 | HC85 | M99 |
| A | Nov. 5 | 0.95 | 0.095 | 0.077 | 0.085 | 0.090 | 7.4 | 7.5 | 0.0126 | 0.0103 | 0.0115 | 0.0122 |
| B | Oct. 14 | 0.85 | 0.090 | 0.070 | 0.077 | 0.082 | 6.65 | 6.1[b] | 0.0120 | 0.0104 | 0.0115 | 0.0122 |
| C | Nov. 16 | 0.88 | 0.076 | | 0.100 | | 6.5 | 6.4[b] | 0.0116 | | | |

[a] MD81, kinetics of *Martin and Damschen* [1981]; HC85, kinetics of *Hoffmann and Calvert* [1985]; M99, kinetics of *Maass et al.* [1999].

[b] R is radius of droplet of average volume at time of maximum LWC.

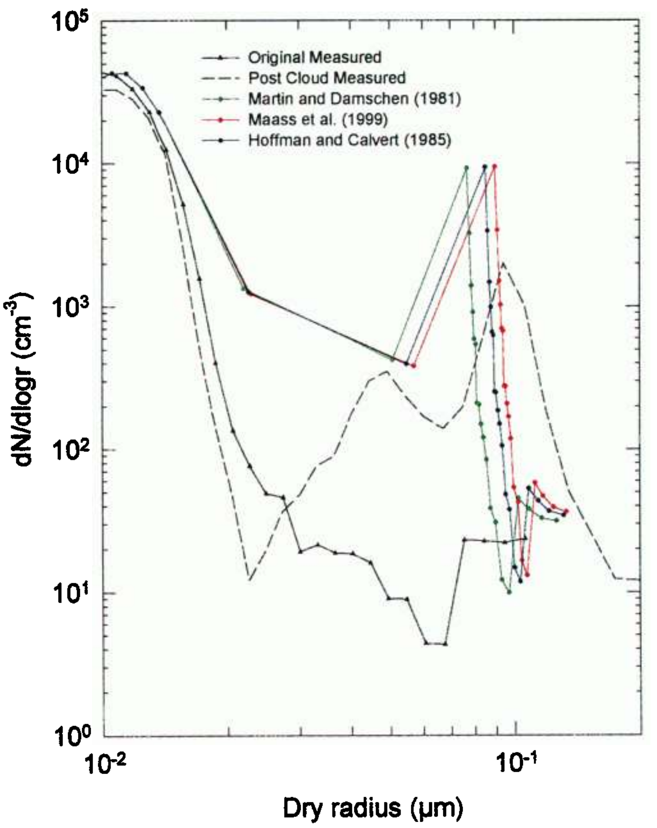

**Plate 3.** Comparison of cloud model predictions of aerosol growth versus the measured growth for three different $SO_2$ - $H_2O_2$ (aq) kinetic formulations, for run A.

2 ppb, $O_3$ = 61 and 64 ppb). However, with similar total pressure expansions and cloud LWC of 0.42 and 0.45 g m$^{-3}$, respectively, the higher concentration of CCN in run E produced a cloud with smaller droplets (PMS-measured peak radii of 6.25 µm for run E versus 7.75 µm for run D).

Growth of residual aerosol was smaller for run E as well, and as *Hoppel et al.* [1994b] showed (beginning with the $SO_2$ - $O_3$ reaction rate equation given in Table 2), the (dry) radius after cloud processing, *r*, is directly proportional to the cloud radius. This can be approximated by

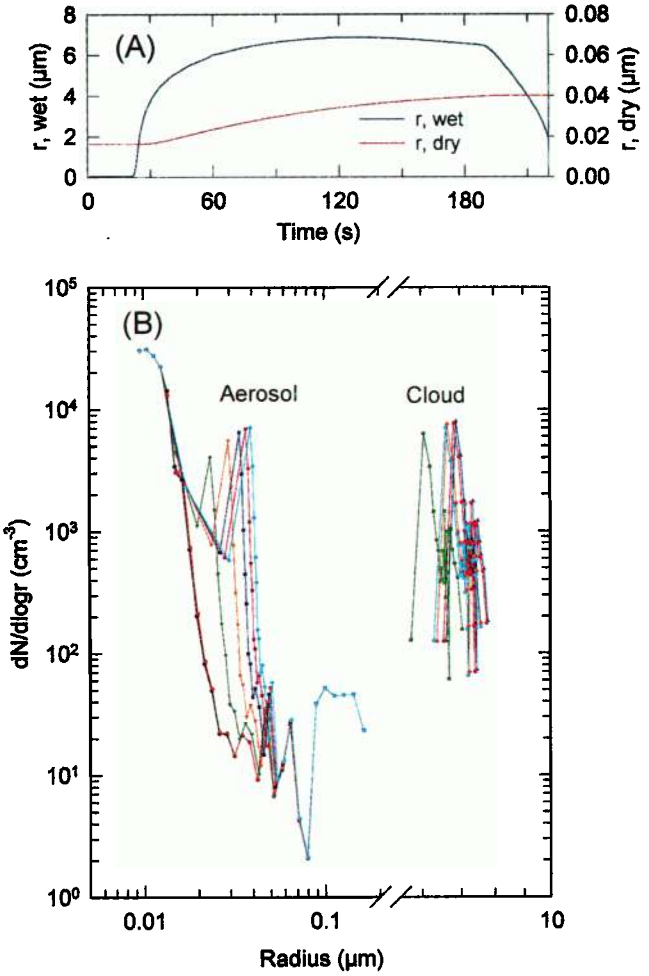

**Plate 4.** Modeling results, run D, $SO_2$ - $O_3$ conversion. (a) Aerosol and cloud droplet radius for the smallest activated size bin, and (b) Cloud droplet and residual dry aerosol size distributions, at 30 s intervals.

$$\frac{r}{R}=\left[1.5\times10^{-5}\,\frac{P_{O_3}P_{SO_2}}{\rho_a^3}\times T\right]^{1/3}, \qquad (19)$$

where *T* is the time in a cloud with droplets of radius *R*. This relation is valid only when the pH of the droplet is greater than

**Table 6.** Experimental Results, $SO_2$ - $O_3$ Cloud Processing

| Run | Date | $SO_2$, ppb | $O_3$, ppb | CCN, cm$^{-3}$ DMA[a] | CCN, cm$^{-3}$ PMS | Maximum LWC, g m$^{-3}$ | Aerosol Radius *r*, µm Initial[b] | Aerosol Radius *r*, µm Final | Cloud Radius *R*, µm | *r/R* | Cloud Duration[c], s | Aerosol ΔVol, µm$^3$ cm$^{-3}$ |
|---|---|---|---|---|---|---|---|---|---|---|---|---|
| D | Nov. 4 | 3.0 | 61 | 270/305 | 300 | 0.42 | 0.016 | 0.068 | 7.75 | 0.0087 | 165 | 0.435 |
| E | Nov. 19 | 2.0 | 64 | 390/410 | 450 | 0.45 | 0.015 | 0.045 | 6.25 | 0.0072 | 130 | 0.183 |
| F | Oct. 13 | 2.8 | 60 | 710 | 675 | 0.35 | 0.026 | 0.049 | 4.9[d] | 0.0101[d] | 210 | 0.347 |
| G | Oct. 21 | 2.0 | 77 | 2810/3630 | 825 | 0.43 | 0.016 | 0.037 | 3.0[d] | 0.0120[d] | 185 | 0.363 |
| H | Nov. 3 | 2.0 | 65 | 840 | 700 | 0.50 | 0.019 | 0.043 | 5.2[d] | 0.0082[d] | 180 | 0.361 |
| I | Nov. 6 | 3.5 | 62 | 1100/1250 | 700 | 0.41 | 0.015 | 0.040 | 4.3[d] | 0.0094[d] | 150 | 0.378 |

[a] Aerosol number concentration in cloud-processed peaks, listed as (peak 1/ peak 1 + peak 2) when necessary.
[b] Rounded to nearest 0.001 µm from DMA bin data.
[c] Time from cloud formation till pressure equalization.
[d] R is radius of droplet of average volume at time of maximum LWC.

**Table 7.** Model Results, $SO_2$ - $O_3$ Cloud Processing

| | | | Final Aerosol Radius *r*, μm | | Aerosol ΔVol, $\mu m^3\ cm^{-3}$ | | Maximum Cloud Droplet *R*, μm | | *r/R* | | |
|---|---|---|---|---|---|---|---|---|---|---|---|
| Run | Date | S, % | Model | Measured | Model | Measured | Model | Measured | Measured | Equation (19) | Modeled |
| D | Nov. 4 | 0.95 | 0.0402 | 0.068 | 0.072 | 0.435 | 6.89 | 7.75 | 0.0087 | 0.0073 | 0.0058 |
| E | Nov. 19 | 0.95 | 0.0357 | 0.045 | 0.067 | 0.183 | 6.41 | 6.25 | 0.0072 | 0.0068 | 0.0056 |
| F | Oct. 13 | 0.50 | 0.0351 | 0.049 | 0.048 | 0.347 | 5.2 | 4.90[a] | 0.0101[a] | | 0.0068 |
| G | Oct. 21 | 0.78 | 0.022 | 0.037 | 0.033 | 0.363 | 3.24 | 3.05[a] | 0.0120[a] | | 0.0068 |
| H | Nov. 3 | 0.72 | 0.0337 | 0.043 | 0.078 | 0.361 | 5.56 | 5.22[a] | 0.0082[a] | | 0.0061 |
| I | Nov. 6 | 0.93 | 0.0285 | 0.040 | 0.072 | 0.378 | 5.2 | 4.28[a] | 0.0094[a] | | 0.0055 |

[a] R is radius of droplet of average volume at time of maximum LWC.

~4.0, where the oxidation of the sulfite ion (term with rate constant $k_2$) is more important than the oxidation of the bisulfite ion ($k_1$). The ninth root relationship indicates that the dependence of *r* (and mass conversion) on $P_{O3}$, $P_{SO2}$, and time in cloud are much weaker than the dependence on *R*.

This ninth root dependence, as compared to only the third root dependence in the case of oxidation by $H_2O_2$, is the result of the strong pH dependence of the $SO_2$ - $O_3$ reaction. Increasing *R* rapidly dilutes the acidity of the droplet and increases the oxidation rate. This dilution effect has a much stronger effect than changing the level of reactants or time in cloud. This is qualitatively seen here in the measured growth of runs D and E, as run E, with smaller cloud droplets, has less residual growth.

According to equation (19), small differences in reactant levels and time in cloud will have little effect on the value of r/R, and therefore this ratio will be used to assess the experimental and modeling results. Comparison of the experimental results with ratios calculated from equation (19) are listed in Table 7, calculated using *R* at the time of maximum LWC and the initial level of $P_{SO2}$ and $P_{O3}$. The use of the maximum value of *R* will overestimate the ratio, as the cloud droplet sizes did not remain fixed, but grew to a maximum and then began to slowly evaporate due to nonadiabatic effects, as shown in Figure 2. However, in spite of this, these overestimated values of r/R were 0.0073 and 0.0068, smaller than the measured growth of 0.0087 and 0.0072, which are greater by 20% and 6%, respectively. Comparisons for runs F-I are not possible without valid cloud droplet size data.

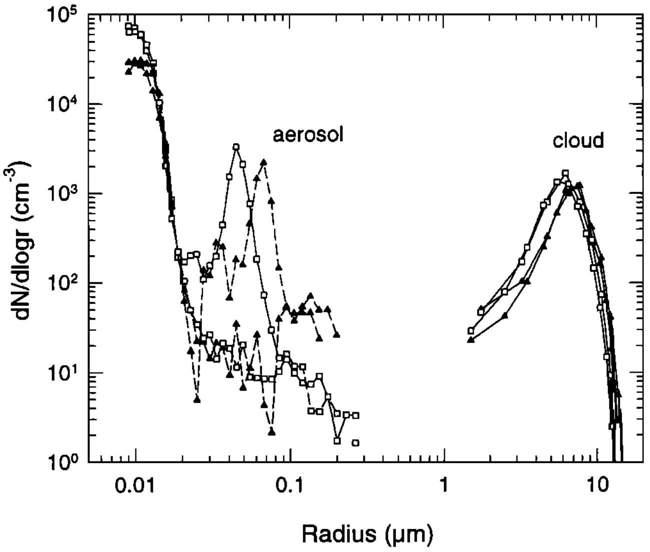

**Figure 5.** Measured aerosol growth from in-cloud conversion via $SO_2$ - $O_3$ (aq) reactions for runs D (solid triangles) and E (open squares) with size distributions for both precloud and postcloud aerosol and for the peak cloud LWC cloud droplet distributions.

### 5.2. Modeling Results

Predictions of growth from calculations made with the cloud microphysical model are compared with measured values in Table 7 for all runs, and model-predicted particle and cloud droplet size distributions are displayed in Plate 4b for run D in 30 s intervals. Plate 4a, comparable to results for $H_2O_2$ in Plate 2a, shows the temporal cloud droplet and residual particle growth for the smallest activated size bin. Self-limited by the decreasing $SO_2$ solubility with decreasing pH, the model predicted particle growth slows quickly after cloud droplet activation, as evident in Plate 4b, with growth of the modal radius predicted to reach only 0.04 μm, significantly less growth than was seen in the $H_2O_2$ runs. Model predicted radial growth in the residual aerosol is only 60% and 80% of that measured for runs D and E, respectively, and is 79%, 71%, 71%, and 60% of the growth measured in the other four runs, as listed in Table 7 and depicted in Figure 6. In terms of normalized growth, r/R, the modeled growth is lower than that observed by 67% and 78% for these two runs, with values of 0.0058 and 0.0056, respectively. As cloud droplet distribution data for the other four runs are not available, the size of the droplet of average volume, or radius of average volume (calculated as maximum LWC/CCN number concentration) is used (these results are also listed in Table 7). For these runs, *r/R* range from 0.0082 to 0.0120, as compared with modeled values from 0.0061 to 0.0068, overall averaging only 66% of the normalized growth (*r/R*) measured in the chamber. Thus normalized radial growth (*r/R*) is predicted to be only 67-78% of that measured.

These results are consistent with previous measurements made at this chamber by *Hoppel et al.* [1994b] under less controlled conditions, where measurements of mass were significantly higher than those estimates from modeling. These

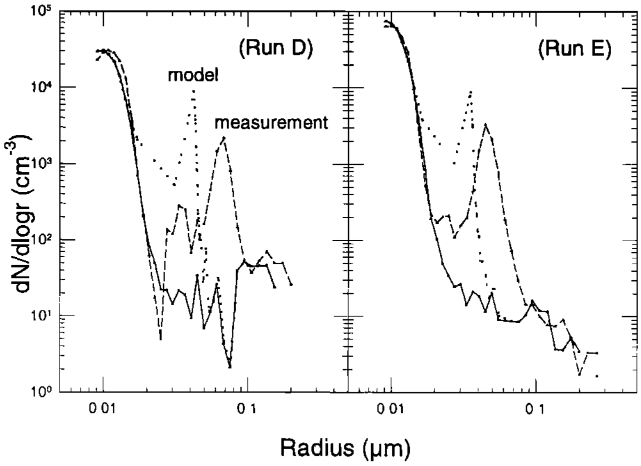

**Figure 6.** Cloud model predictions versus the measured growth for $SO_2$ - $O_3$ experiments. (a) Run D and (b) run E with dotted and dashed lines representing the modeled and measured cloud-processed dry aerosol size distribution, respectively, and the solid line representing the original aerosol SD.

results show that this discrepancy has not been eliminated here through the use of additional experimental instrumentation, nor has it been resolved through the use of a vastly improved cloud chemistry model. Its source is still unknown, although discussion of possible explanations follows.

### 5.3. Discussion: $SO_2$ - $O_3$ Oxidation

Modeling was conducted to determine the level of changes to the chemical rate constants that are necessary for the model to account for the measured growth in the $SO_2$ - $O_3$ experiments. As determined from agreement in the r/R values, an increase of 16 times the rate constant for $O_3$ - $SO_3^{2-}$ reaction ($k_2$ in Table 3), from 1.5 ($10^9$) to 2.4 ($10^{10}$) $M^{-2}$ $s^{-1}$, is required for the model predictions to match the measurements for run D, and of 5 times for agreement for run E. Similarly, increases of 175 and 75 times the value used for $k_1$ ($O_3$ - $HSO_3^-$) are needed, assuming no changes to the other rate constants. Changes to the rate constant for oxidation of $SO_2$ (aq) ($k_0$) were not determined. (The different factors for runs D and E reflect that different amounts of relative growth were measured for these two runs: *r/R* for run D was 0.0087, while for run E it was 0.0072).

Thus, if the measurement errors in the rate expressions were responsible for the discrepancy between the measurements and modeling, the error in the rate constants would, at a minimum, be a factor of 5. It seems unlikely that the error in these measured rate constants could be this large, and therefore also unlikely that errors in the rate expressions themselves responsible for the differences measured here.

Assuming then, that any errors in the modeling and chemical kinetics are not responsible for these discrepancies, the possibility of contamination or other chemical mechanisms that could explain the measured conversion should be examined. As the $SO_2$ - $O_3$ reaction is sensitive to pH, anything affecting the pH of the cloud droplets could have a large impact on the amount of S(VI) produced. Aerosol growth measured during second and third cloud cycles (performed subsequent to the initial cloud cycle on the residual, cloud- processed aerosol) suggest that trace amounts of $NH_3$ (or some other base) were present in the chamber at levels that could increase model-predicted aerosol growth enough to bring agreement with the measurements.

In addition to the cloud cycles reported in Table 6, second and third clouds were formed during each experimental run. Typically, the second cloud showed little additional growth in the cloud-processed aerosol mode, a consequence of the $SO_2$ - $O_3$ reaction rate decreasing with decreasing pH. Model-predicted cloud droplet pH values near the end of the first cloud were 4.9 and 4.2, respectively, and particle growth at these pH values on the timescale of these clouds is negligible. The reactants, however, were not depleted significantly by the cloud processing. During two experiments (runs F and H, October 13 and November 3), a more rapid pressure expansion during the second cloud cycle produced a greater chamber supersaturation, activating additional particles (as compared to the first cloud). CCN number concentrations for these two runs, as determined from the postcloud DMA size distributions, were 700-800 cm$^{-3}$ during first cloud but 2000-3000 cm$^{-3}$ during the second cloud. These additional cloud droplets created a distinct, secondary cloud-processed aerosol mode located at smaller radius than the first (original) mode, with the newly activated particles growing from <0.02 µm to near 0.03 µm ($r_{dry}$), as displayed in Figure 7 for run F.

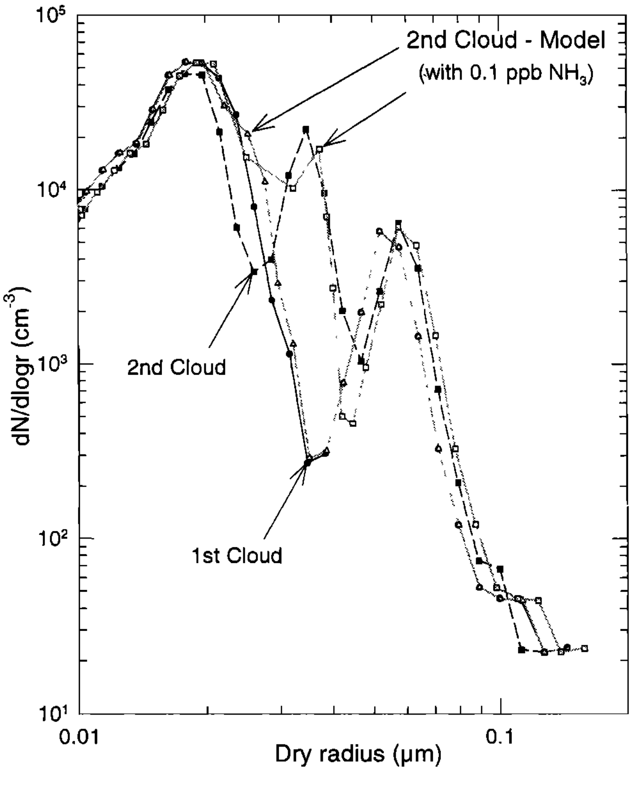

**Figure 7.** Measured aerosol growth from $SO_2$ - $O_3$ oxidation for run F , with results shown from processing by two consecutive clouds for each run. Note the second cloud (first cloud with solid line, second cloud with dashed line) activated more particles and produced a second cloud-processing peak. Model-predicted aerosol growth during the second cloud of run F, with and without the addition of 0.1 ppb $NH_3$, are displayed as labeled (the grey lines represent the model results). The addition of a trace amount of $NH_3$ reproduces the measured growth of the second peak, while not affecting growth in the primary mode.

Modeling of these clouds, however, does not reproduce this growth. Run F modeling results are shown in Figure 7. Although the model reproduces the microphysics of these clouds from the second cycle and activates the new particles into a bimodal cloud droplet distribution, very little cloud processing growth of these new CCN is predicted, much less than that measured as shown in Figure 7. This is consistent with the smaller size of the cloud droplets: as the pressure expansion (and therefore total cloud LWC) is similar to that of the first cloud, the larger number of CCN yields a cloud with smaller droplets. Peak model-predicted cloud radii for the newly activated particles are at 3.5 and 3.3 μm for runs F and H, respectively (there are no valid PMS-OPC measurements of the cloud droplet distribution for these runs), and the model-predicted pH of these droplets is 4.7 and 5.0, respectively, too low to support significant amounts of growth in the 3-4 min of the lifetime of the cloud (the $SO_2$ - $O_3$ reaction rate in 3.3 μm droplets (pH = 5) is ~100 times lower than the reaction rate for a 6.5 μm droplet (pH = 6)).

However, including trace amounts of $NH_3$ in the modeling does predict growth in the secondary peak comparable to the measurements, while not affecting the primary mode, as displayed in Figure 7. This can be explained through the effect of pH on the $SO_2$ - $O_3$ reaction rate. Simple calculations made for a 3.6 μm droplet formed on 0.02 μm (newly activated particles) and 0.1 μm (original, primary mode of cloud processed particles) $H_2SO_4$ particles in equilibrium with 0.1 ppb $NH_3$ (g) yield droplet pH values of 6.2 and 4.1, respectively. The equivalent $SO_2$ - $O_3$ oxidation rate at pH = 6.2 is 4 orders of magnitude greater than that at a pH of 4.1. Model results for run F with 0.1 ppb $NH_3$, showing agreement with measurements, are displayed in Figure 7. Similarly (but not shown), the addition of 0.15 ppb of $NH_3$ to run H produces excellent agreement with the measurements.

Extending this analysis shows that similar levels of $NH_3$ can reproduce the measured growth in the first cloud cycles as well. Modeling results of runs D and E (November 4 and 19) with the inclusion of 0.15 and 0.05 ppb $NH_3$ yield, respectively, r/R values of 0.0089 (102% measured) and 0.0073 (101%), showing excellent agreement with the measurements. Figure 8 displays these results for run D, comparing the modeling results with and without 0.15 ppb $NH_3$ with the measurements. Similarly, the amount of $NH_3$ in the modeling runs needed to reproduce the measured r/R ratios for the other runs (within 5%) ranged from 0.1 to 0.15 ppb. Concentrations of $NH_3$ at these levels are common in the atmosphere, especially over continental areas, and the results here emphasize the importance of explicitly including $NH_3$ in modeling studies of particle growth by cloud processing of $SO_2$ by $O_3$.

Thus trace amounts of ammonia present in the chamber may be responsible for the discrepancy between the modeling and measurements noted above and in the past [*Hoppel et al.*, 1994b]. However, no measure of $NH_3$ at these levels were made during these experiments, and such a conclusion is therefore not possible. The discrepancy may likely be the result of other factors not yet considered.

## 6. Summary

Aqueous-phase oxidation of $SO_2$ by $O_3$ and $H_2O_2$ in cloud droplets and the resulting growth of the CCN by residual S(VI) was measured in experiments conducted at the Calspan environmental chamber. Clouds with LWC ranging from 0.3-0.6 g $m^{-3}$, typical LWC values of stratus and stratocumulus clouds, were formed and held for 3-5 min, and growth of the residual aerosol was measured from changes to the size distribution measured by the NRL DMA after the cloud. Simulation of cloud formation and cloud chemistry with a computer model showed that aerosol growth from the $SO_2$ - $H_2O_2$ reaction is best predicted using the kinetic formulation of *Maass et al.* [1999], and agreement between modeling predictions and the measurements was within 3%. Modeling results using kinetics from *Martin and Damschen* [1981] showed agreement within 9%, and results from kinetics of *Hoffmann and Calvert* [1985] were within 18% of the measurements.

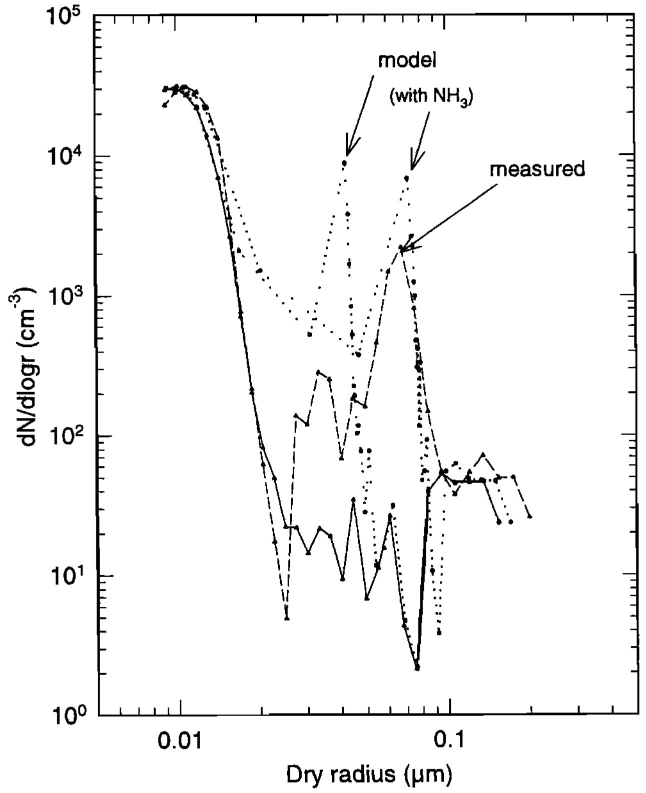

**Figure 8.** Model-predicted and measured aerosol growth, run D, both with and without 0.1 ppb of $NH_3$ (the dotted lines represent the model results, the dashed line the measured result, and the solid line is the original SD). The addition of $NH_3$ increases the model-predicted growth to essentially equal the measured growth.

Measurements of aerosol growth from the $SO_2$ - $O_3$ reaction were (1) greater than model predictions and (2) inconsistent based upon cloud and reactant conditions. Uncertainties in the kinetic rate constants are unlikely to account for the differences, as each rate constant would have to be increased by a factor >5. Measurements of secondary cloud processing modes suggest the presence of $NH_3$ at levels <0.2 ppb could account for all the measured growth, and contamination would explain the different rates measured on different days. However, no measurements of $NH_3$ below 1 ppb were made, and thus the source of the excess conversion/growth is still an open question.

**Acknowledgments.** This work was supported by the Office of Naval Research and the National Oceanographic Participation Program, Coastal and Marine Aerosol Transformation Processes Experiment.

This work also constitutes a contribution to the International Global Atmospheric Chemistry (IGAC) core project of the International Geosphere-Biosphere Programme (IGBP).

## References

Baumgardner, D., and M. Spowart, Evaluation of the Forward Scattering Spectrometer Probe, part III,Time response and laser inhomogeneity limitations, *J. Atmos. Oceanic Technol.*, *7*, 666-672, 1990.

Botha, C. F., J. Hahn, J. J. Pienaar, and R. Van Eldik, Kinetics and mechanism of the oxidation of sulfur(IV) by ozone in aqueous-solutions, *Atmos. Environ.*, *28*, 3207-3212, 1994.

Bower, K. N., T. A. Hill, H. Coe, and T. W. Choularton, $SO_2$ oxidation in an entraining cloud model with explicit microphysics, *Atmos. Environ., Part A*, *25*, 2401-2418, 1991.

Bower, K. N., et al., Observations and modelling of the processing of aerosol by a hill cap cloud, *Atmos. Environ.*, *31*, 2527-2543, 1997.

Bower, K. N., A. Jones, and T. W. Choularton, A modelling study of aerosol processing by stratocumulus clouds and its impact on general circulation model parameterisations of cloud and aerosol, *Atmos. Res.*, *50*, 317-344, 1999.

Bradbury, C., et al., Modelling of aerosol modification resulting from passage through a hill cap cloud, *Atmos. Res.*, *50*, 185-204, 1999.

Chylek, P., Extinction and liquid water content of fogs and clouds, *J. Atmos. Sci.*, *35*, 296-300, 1978.

Dye, J. E., and D. Baumgardner, Evaluation of the Forward Scattering Spectrometer Probe, part 1, Electronic and optical studies, *J. Atmos. Oceanic Technol.*, *1*, 329-344, 1984.

Fitzgerald, J. W., Dependence of supersaturation spectrum of CCN on aerosol size distribution and composition, *J. Atmos. Sci.*, *30*, 628-634, 1973.

Fitzgerald, J. W., A study of the initial phase of cloud droplet growth by condensation: Comparison between theory and observation, Ph.D. thesis, Dep. of Geophys. Sci., Univ. of Chicago, Chicago, Ill., 1972.

Giauque, W. F., E. W. Hornung, J. E. Kunzler, and T. R. Rubin, The thermodynamic properties of aqueous sulfuric acid solutions and hydrates from 15 to 300 deg K, *J. Am. Chem Soc*, *34*, 62-82, 1960.

Hansen, A. D. A., W. H. Benner, and T. Novakov, Sulfur-dioxide oxidation in laboratory clouds, *Atmos. Environ., Part A*, *25*, 2521-2530, 1991.

Hegg, D. A., P. V. Hobbs, and L. F. Radke, Observations of the modification of cloud condensation nuclei in wave clouds, *J. Rech. Atmos.*, *14*, 217-222, 1980.

Hinds, W. C., *Aerosol Technology - Properties, Behavior, and Measurement of Airborne Particles*, John Wiley, New York, 1982.

Hoffmann, M. R., and J. G. Calvert, Chemical transformation modules for eularian acid deposition models, vol. 2, The aqueous-phase chemistry, *Rep. EPA/600/3-85/017*, U.S. Environ. Prot. Agency, Research Triangle Park, N. C., 1985.

Hoppel, W. A., and G. M. Frick, Submicron aerosol size distributions measured over the tropical and south pacific, *Atmos. Environ., Part A*, *24*, 645-659, 1990.

Hoppel, W. A., G. M. Frick, and R. E. Larson, Effect of nonprecipitating clouds on the aerosol size distribution in the marine boundary layer, *Geophys. Res. Lett.*, *13*, 125-128, 1986.

Hoppel, W. A., G. M. Frick, J. Fitzgerald, and R. E. Larson, Marine boundary layer measurements of new particle formation and the effects nonprecipitating clouds have on aerosol size distribution, *J. Geophys. Res.*, *99*, 14,443-14,459, 1994a.

Hoppel, W. A., G. M. Frick, J. W. Fitzgerald, and B. J. Wattle, A cloud chamber study of the effect that nonprecipitating water clouds have on the aerosol size distribution, *Aerosol Sci. Technol.*, *20*, 1-30, 1994b.

Hoppel, W. A., G. M. Frick, and J. W. Fitzgerald, Deducing droplet concentration and supersaturation in marine boundary layer clouds from surface aerosol measurements, *J. Geophys. Res.*, *101*, 26,553-26,565, 1996.

Hoppel, W., G. Frick, P. Caffrey, L. Pasternack, T. Albrechcinski, J. Ambrusko, W. Sullivan, D. Hegg, and S. Gao, Report on the characterization of Calspan's 600 $m^3$ chamber in preparation for the NOPP aerosol processes experiments, *Rep. NRL/MR/6110-99-8370*, Nav. Res. Lab., Washington, D. C., 1999.

Jayne, J. T., P. Davidovits, D. R. Worsnop, M. S. Zahniser, and C. E. Kolb, Uptake of SO2(g) by aqueous surfaces as a function of pH - The effect of chemical reaction at the interface, *J. Phys. Chem.*, *94*, 6041-6048, 1990.

Lide, D. R. (Ed.), *CRC Handbook of Chemistry and Physics*, CRC Press, Boca Raton, Fla., 1990.

Liu, X. H., and W. Seidl, Modeling study of cloud droplet nucleation and in-cloud sulfate production during the sanitation of the atmosphere (Sana) 2 campaign, *J. Geophys. Res.*, *103*, 16,145-16,158, 1998.

Lowe, B. J., and J. M. Ficke, The computation of saturation vapor pressure, *Tech. Pap. 4-74*, Environ. Res. Pred. Facil., Nav. Postgrad. Sch., Monterey, Calif., 1974.

Luke, W. T., Evaluation of a commercial pulsed fluorescence detector for the measurement of low-level $SO_2$ concentrations during the gas-phase sulfur intercomparison experiment, *J. Geophys. Res.*, *102*, 16,255-16,265, 1997.

Maass, F., H. Elias, and K. J. Wannowius, Kinetics of the oxidation of hydrogen sulfite by hydrogen peroxide in aqueous solution: Ionic strength effects and temperature dependence, *Atmos. Environ.*, *33*, 4413-4419, 1999.

Martin, L. R. and D. E. Damschen, Aqueous oxidation of sulfur-dioxide by hydrogen-peroxide at low pH, *Atmos. Environ.*, *15*, 1615-1621, 1981.

O'Dowd, C. D., J. A. Lowe, and M. H. Smith, Observations and modelling of aerosol growth in marine stratocumulus - Case study, *Atmos. Environ.*, *33*, 3053-3062, 1999.

Pruppacher, H. R., and J. D. Klett, *Microphysics of Clouds and Precipitation.*, Kluwer Acad., Norwell, Mass., 1997.

Sander, R., and P. J. Crutzen, Model study indicating halogen activation and ozone destruction in polluted air masses transported to the sea, *J Geophys. Res*, *101*, 9121-9138, 1996.

Schwartz, S. E., Mass-transport limitation to the rate of in-cloud oxidation of $SO_2$: Re-examination in the light of new data, *Atmos. Environ.*, *22*, 2491-2499, 1988.

Seinfeld, J. H., and S. N. Pandis, *Atmospheric Chemistry and Physics - From Air Pollution to Climate Change*, John Wiley, New York, 1998.

Tremblay, A., and H. Leighton, A 3-dimensional cloud chemistry model, *J. Clim. Appl. Meteorol.*, *25*, 652-671, 1986.

Wells, M., T. W. Choularton, and K. N. Bower, A modelling study of the interaction of ammonia with cloud, *Atmos. Environ.*, *32*, 359-363, 1998.

---

T. Albrechcinski and J. Ambrusko, Calspan-University of Buffalo Research Center, Buffalo, NY 14225.

P. Caffrey, J. Fitzgerald, G. Frick, and W. Hoppel, Naval Research Laboratory, Code 7228, Washington, DC 20375 (Peter.Caffrey@nrl.navy.mil)

S. Gao and D. Hegg, University of Washington, Department of Atmospheric Sciences, Seattle, WA 98195.

R. Leaitch and N. Shantz, Meteorological Service of Canada, Downsview, Ontario, Canada MH3 5T4.

L. Pasternack, Chemistry Division, Naval Research Laboratory, Code 6111, Washington, DC 20375.

(Received September 7, 2000; revised December 1, 2000; accepted December 5, 2000.)